Joule

CellPress

Article

Bayesian learning for rapid prediction of lithium-ion battery-cycling protocols

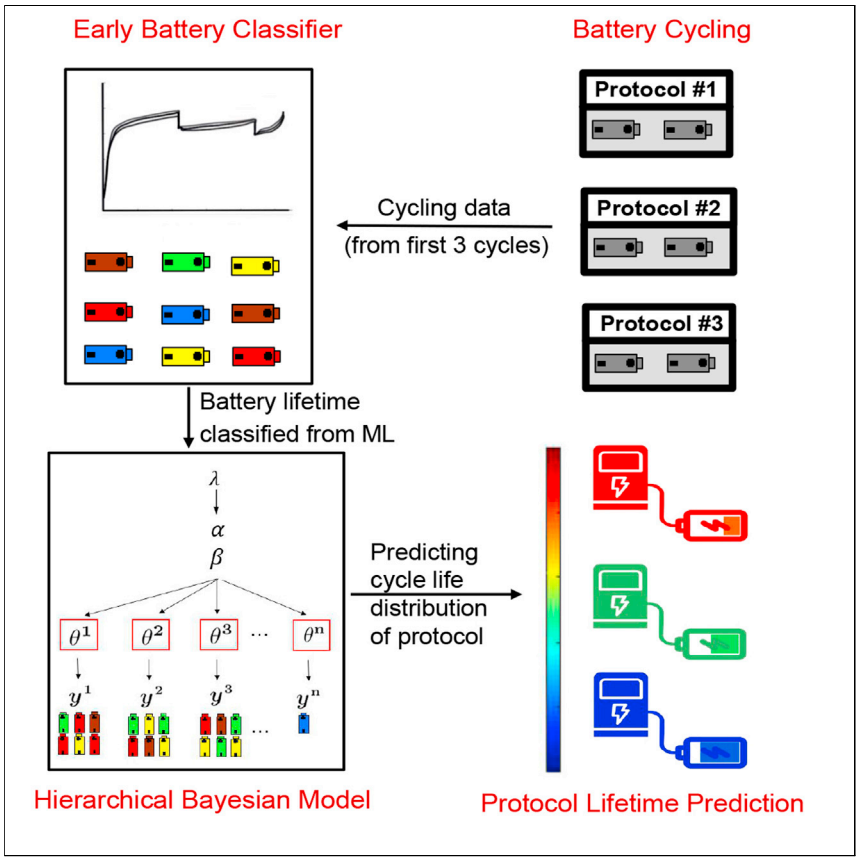

Developing advanced lithium-ion batteries requires optimizing performance across parameter spaces with extremely high dimensionality, long testing times, and high variability between cells, particularly in early development. A machine learning methodology is developed for accelerating the design of cycling protocols, with reduced experimental costs of testing time and cells, by providing accurate evaluation of cycling protocols using very few cycles and cells.

Benben Jiang, William E. Gent, Fabian Mohr, ..., Stefano Ermon, William C. Chueh, Richard D. Braatz

braatz@mit.edu

Highlights

A methodology is proposed for predicting cycle life for new cycling protocols

Accurate predictions are obtained after only a few measurements

This approach can considerably reduce experimental costs in terms of cells and time

Effectiveness is demonstrated for both LFP/graphite and NMC/graphite cells

Jiang et al., Joule 5, 3187–3203
December 15, 2021 © 2021 Elsevier Inc.
https://doi.org/10.1016/j.joule.2021.10.010

Joule

CellPress

Article

Bayesian learning for rapid prediction of lithium-ion battery-cycling protocols

Benben Jiang,[1] William E. Gent,[2] Fabian Mohr,[3] Supratim Das,[3] Marc D. Berliner,[3] Michael Forsuelo,[3] Hongbo Zhao,[3] Peter M. Attia,[2] Aditya Grover,[4] Patrick K. Herring,[5] Martin Z. Bazant,[3] Stephen J. Harris,[6] Stefano Ermon,[4] William C. Chueh,[2] and Richard D. Braatz[3,7,*]

SUMMARY

Advancing lithium-ion battery technology requires the optimization of cycling protocols. A new data-driven methodology is demonstrated for rapid, accurate prediction of the cycle life obtained by new cycling protocols using a single test lasting only 3 cycles, enabling rapid exploration of cycling protocol design spaces with orders of magnitude reduction in testing time. We achieve this by combining lifetime early prediction with a hierarchical Bayesian model (HBM) to rapidly predict performance *distributions* without the need for extensive repetitive testing. The methodology is applied to a comprehensive dataset of lithium-iron-phosphate/graphite comprising 29 different fast-charging protocols. HBM alone provides high protocol-lifetime prediction performance, with 6.5% of overall test average percent error, after cycling only one battery to failure. By combining HBM with a battery lifetime prediction model, we achieve a test error of 8.8% using a single 3-cycle test. In addition, the generalizability of the HBM approach is demonstrated for lithium-manganese-cobalt-oxide/graphite cells.

Context & scale

Advancing lithium-ion battery technology requires the optimization of cycling protocols. A machine learning methodology is developed to accelerate the design of cycling protocols, with reduced experimental costs of testing time and cells, by providing accurate evaluation of cycling protocols using very few cycles and cells. The approach is able to obtain accurate predictions after only a few measurements, by explicitly accounting for cell-to-cell variability and battery lifetime prediction uncertainties. This methodology can be embedded into an optimization algorithm over the battery operating parameters. This optimization task is becoming increasingly important as next-generation electrode and electrolyte chemistries (e.g., Si anodes, S cathodes, and solid-state electrolytes) with unfamiliar electrochemical behaviors near commercial deployment.

INTRODUCTION

The high energy and power densities of lithium-ion batteries have resulted in their ubiquity in a wide range of applications, including cellphones, laptops, automotive vehicles, and smart grids.[1–5] The optimization of cycling protocols, which affect the utility and lifetime of the batteries, is key to the development of advanced batteries for these applications. For example, multistep fast-charging protocols may enable shorter charging times without sacrificing cycle life by minimizing current-induced degradation.[6–8,9] Similarly, more complex formation protocols may reduce the formation time while increasing the cycle life and/or safety by modulating the deposition, chemistry, and morphology of the solid-electrolyte interphase.[9,10] As new electrode chemistries, such as silicon-alloy anodes and Ni-rich or over-lithiated oxide cathodes near commercial deployment, there is a need to develop and rapidly evaluate new cycling protocols that minimize electrochemically induced degradation while maximizing performance.

Such optimizations are expensive and time consuming due to the (1) high dimensionality of the parameter space, (2) high manufacturing variability, and (3) long testing times.[11–13] The dimensionality is high, in that the size of the parameter space of conceivable protocols is large relative to the number of experimental evaluations that can be realistically carried out. The manufacturing variability is high, in that each combination of parameters can exhibit significant variability in battery lifetime (i.e., high variability between cells) due

to exogenous factors, particularly during early development of new technologies and materials. In addition, testing each protocol is time intensive, as cells are designed to last several years and hundreds to thousands of charge/discharge cycles. Current methods to circumventing these challenges include conducting accelerated cycle-life tests by either cycling under extreme conditions (high temperatures and rates) or predicting the lifetime based on the electrochemical response in early cycles. In both cases, extensive repetitive testing is required to account for cell-to-cell variability and/or errors in early lifetime prediction. Therefore, methods to efficiently address these challenges are of crucial importance in enabling the rapid advancement of battery technologies for next-generation applications.

Recent interest has focused on employing machine learning techniques to accelerate a variety of similar optimization and evaluation tasks, including identification of chemical synthesis routes,[14,15] device modeling for photovoltaic materials,[16] and materials discovery for energy storage.[17–20] In general, machine learning enables the development of predictive or descriptive models based on training data in the absence of a complete understanding of the underlying physics, making it also well suited to the present challenge of battery-cycling protocol evaluation. For example, our previous work[2] demonstrated that machine learning models are able to accurately classify batteries into high- and low-cycle-life groups after only 5 cycles, cutting down testing time by several orders of magnitude and directly addressing the challenge of long testing times in battery protocol optimization. However, such approaches do not explicitly account for cell-to-cell variability, thus achieving sufficient confidence in the prediction of protocols (rather than individual cells under test) still required multiple repeated measurements even when using this accelerated approach.[2]

In this work, we develop data-driven models to conduct rapid prediction of lithium-ion battery-cycling protocols using only a single accelerated experimental test lasting only 3 cycles, by combining hierarchical Bayesian model (HBM) methods with a minimax probability machine for battery lifetime prediction. This approach reduces both the testing time and the total number of tests required for iterative cycling protocol optimization, resulting in a total test time reduction of over an order of magnitude compared even with our previous data-driven accelerated approach.[9] The HBM learns both (1) the lifetime distribution of each cycling protocol and (2) the abstract knowledge describing the degree of cell-to-cell lifetime variability among different protocols, as well as overall lifetime distribution for protocols (see Figure 1), which enables the model to infer the performance of new cycling protocols from very few measurements. The approach is demonstrated for a dataset of lithium-iron-phosphate (LFP)/graphite cells from Severson et al.[2] and Attia et al.[9] consisting of 29 different fast-charging protocols with 113 cells whose cycle lives range from 500 to 1,200, with end of life defined as 20% degradation from nominal capacity. After learning from a subset of the data, the HBM methodology alone provides high protocol prediction performance, with 5.7% of a best test average percent error and with 6.5% of overall test error for lifetime prediction of any new cycling protocols, after only one full-cycle-life test with the new cycling protocol. By combining the HBM approach with the battery lifetime prediction model, we achieve a test error of 8.8% for the prediction of new cycling protocol-lifetime after only a single 3-cycle test—a test time reduction of more than 99% compared with a full cycle-life test. In addition, the proposed HBM approaches are demonstrated for a dataset of lithium-manganese-cobalt-oxide (NMC)/graphite cells, providing nearly a factor of two higher accuracy in protocol-lifetime prediction than the benchmarking single-level prediction method,[21] using only a single 3-cycle test.

[1]Department of Automation, Tsinghua University, Beijing 100084, China

[2]Department of Materials Science and Engineering, Stanford University, Stanford, CA 94305, USA

[3]Department of Chemical Engineering, Massachusetts Institute of Technology, Cambridge, MA 02139, USA

[4]Department of Computer Science, Stanford University, Stanford, CA 94305, USA

[5]Toyota Research Institute, Los Altos, CA 94022, USA

[6]Materials Science Division, Lawrence Berkeley National Laboratory, Berkeley, CA 94720, USA

[7]Lead contact

*Correspondence: braatz@mit.edu

https://doi.org/10.1016/j.joule.2021.10.010

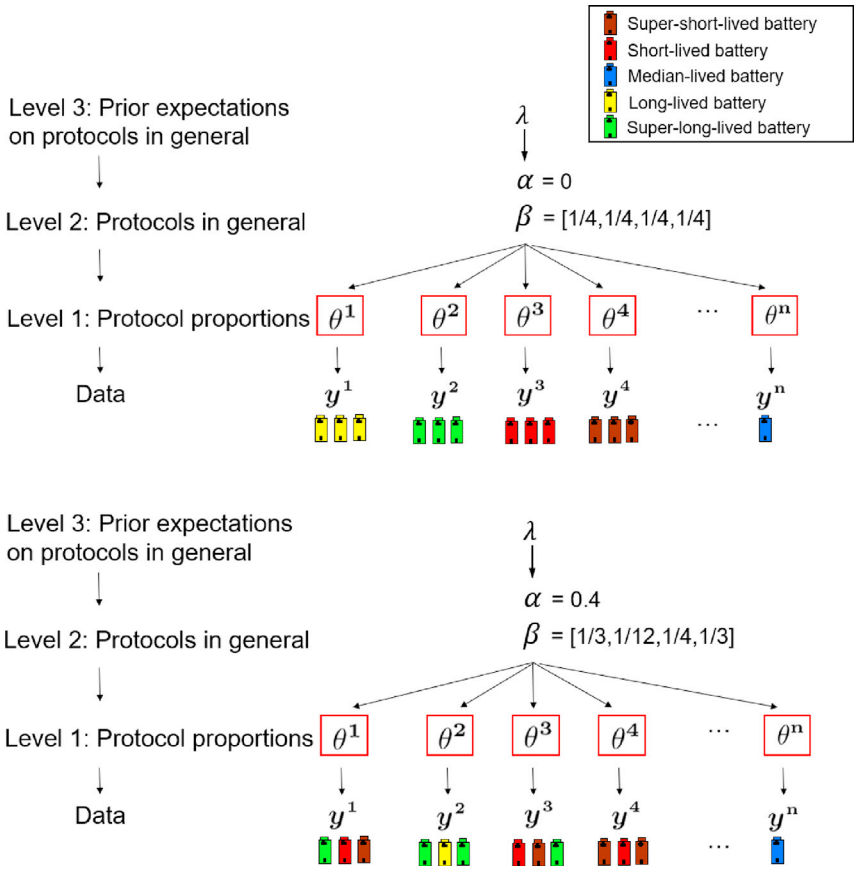

Figure 1. Illustration of hierarchical Bayesian model based on batteries with various cycle lives from different cycling protocols (different colors indicate different battery lifetime groups)

Suppose that *S* is a stack containing many cycling protocols. We sample several protocols and discover that some protocols contain short-lived (red) and super-long-lived (green) batteries, and others contain long-lived (yellow) and super-short-lived (brown) batteries. We now meet a new cycling protocol—protocol n—and draw a single sample from the protocol and observe that the sample is a median-lived (blue) battery. We are interested in the ability to predict the battery lifetime distribution (i.e., $\boldsymbol{\theta}^n$) of the new cycling protocol. On its own, a single draw provides little information about the new protocol, but experience with previous protocols can provide more information for the inference. For example, (A) the lifetime of batteries in each cycling protocol are uniform (i.e., $\alpha = 0$), which endorses the hypothesis H that the lifetime of all batteries from this new protocol n are median lived (blue), and (B) for the case of each protocol possessing a large variability of battery lifetime, the information α and $\boldsymbol{\beta}$ at level 2—in which α is the overall degree of cell-to-cell variability and $\boldsymbol{\beta}$ is the overall lifetime distribution across all protocols—learned from previous protocols is critical for predicting the lifetime distribution (i.e., $\boldsymbol{\theta}^n$) of a new protocol using only few samples (e.g., only one sample).

In past work,[2,9] we demonstrated the potential of machine learning methods for accelerating the optimization of battery operating parameters by reducing the testing times through early prediction of failure and efficiently navigating large parameter spaces, focusing on (1) and (3) mentioned earlier. In contrast, this article considers a different problem in which a method is proposed to accelerate testing by combining early battery lifetime prediction with a HBM to "rapidly predict performance distributions without the need for extensive repetitive testing," simultaneously addressing (2) and (3) mentioned earlier via two advances: (1) HBM is able to obtain accurate predictions after only a few measurements, by explicitly taking into account cell-to-cell variability and battery lifetime prediction uncertainties even when these uncertainties are large; (2) we achieve an additional order of

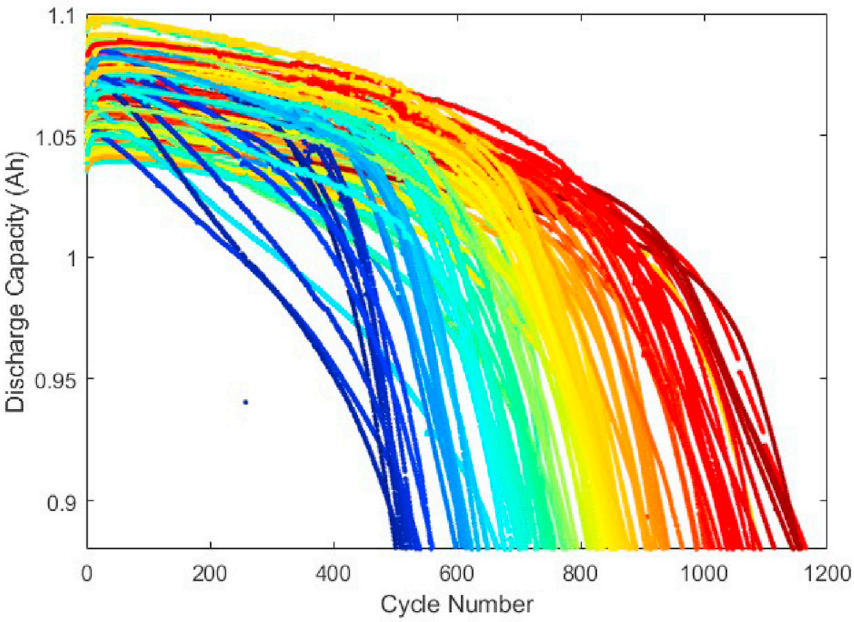

Figure 2. Discharge capacity for all the LFP/graphite cells used in the article
The color of each curve is scaled by the battery's cycle life.

magnitude reduction in testing time compared with lifetime prediction alone, by virtue of relaxing the accuracy required from the early lifetime prediction, and minimizing the need for repeated testing.

Machine learning approach

We use an HBM approach to construct a model for rapid prediction of cycling protocols. As noted earlier, we use HBMs[21,22] to capture the abstract knowledge that describes cell-to-cell lifetime variability among cycling protocols through the learning of hyper-parameters at several levels of abstraction. We provide an informal introduction to this modeling approach, leaving technical details of machine learning model development in the computational section.

Hierarchical learning and inference are often employed in human learners when the training data are very sparse. Just a single example is often sufficient for people to grasp a new category and make meaningful generalizations to novel instances, and accuracy typically asymptotes after just three or four examples.[23,24] Higher levels of abstract knowledge have been observed to play a central role in humans when generalizing successfully from just a few examples.[22,24] For example, a learner may recognize attributes that vary significantly between categories, as well as features that tend to be homogeneous within categories. This more abstract knowledge supports *higher order* generalizations about categories that the person has never seen, which allows a reasonable assessment of an entirely new situation from only one example of a new instance.[25]

Since higher order abstract knowledge is crucial for many human inferences, researchers have explored how this knowledge might be learned. HBMs have been reported to acquire such knowledge.[21] In the HBM framework, the learning of abstract knowledge can be modeled as the learning of hyper-parameters. HBMs have been developed that acquire high-order knowledge for effective learning and inference in many domains. For example, a hierarchical model has been used to discover

whether a corpus of child-directed speech is better described by a regular or a context-free grammar.[26] Discovering abstract properties of the underlying grammar can help language learners zero in on a specific grammar that accounts well for the data that they have observed. In addition, HBM has been adopted for learning causal relations.[27,28] Knowledge about causal types (e.g., diseases and symptoms) and relationships between these types (diseases cause symptoms) has served as useful constraints on causal learning.[27,28] An HBM has been demonstrated that uses raw co-occurrence data to discover abstract knowledge about causal types.[27] In the field of ecology, it is critical to understand how levels of population organization contribute to population niche width.[29] A hierarchical Bayesian-based isotope mixing model has been used to quantify inter- and intra-population niche variability and improved isotope niche width analysis by quantitatively assessing the variability among individuals and across levels of population organization.[29]

In general, the objective of HBM approaches is to model the hierarchical structure in a dataset and draw inferences using Bayesian methods. In our case, the data are battery lifetime observations of cycling protocols ($\boldsymbol{y}^i$ indicates the battery lifetime observations from cycling protocol i) and we are interested in predicting the lifetime distribution (i.e., $\boldsymbol{\theta}^n$) of a new cycling protocol—protocol n—using only few measurements (see Figure 1; computational for more details).

To conduct such inference, knowledge is learned at two levels of the hierarchy, as shown in Figure 1. One of them is the concrete (level 1) knowledge about the lifetime distribution of each training cycling protocol ($\boldsymbol{\theta}^i$ indicates the lifetime distribution for the *i*th protocol), which explains the data and supports the ability of protocol inference. The other is the abstract (level 2) knowledge that describes the knowledge of lifetime variability among protocols and overall lifetime distribution for these protocols. The level-2 knowledge can be represented using two parameters α and $\boldsymbol{\beta}$ (see Equations 6 and 7). Intuitively, α captures the extent to which the battery lifetimes in each protocol tend to be uniform (namely, the degree of cell-to-cell lifetime variability), and $\boldsymbol{\beta}$ indicates the average lifetime distribution across all cycling protocols. This high-order abstract knowledge is what allows the model to form a reasonable prototype of a new kind of cycling protocol from only a few observations.[22,23]

The objective of HBM is to compute the posterior distribution $p(\alpha, \boldsymbol{\beta}, \{\boldsymbol{\theta}^i\} | y)$: in other words, the objective is to simultaneously obtain level-2 knowledge about α and $\boldsymbol{\beta}$ and level-1 knowledge about the lifetime distribution $\boldsymbol{\theta}^i$, $i = 1, 2, \ldots$, of each individual protocol. Inferences about $\boldsymbol{\theta}^i$, the battery lifetime distribution of protocol i, can be marginalized out of the posterior distribution over (α, $\boldsymbol{\beta}$) (see Equation 8). The inference can be implemented in several ways and the inference scheme adopted here calculates the mean prediction.

The training dataset (21 different cycling protocols tested with varying repetitions across 73 batteries) is used to train the HBM model to learn the level-1 knowledge of $\boldsymbol{\theta}^i$, as well as the level-2 knowledge of (α, $\boldsymbol{\beta}$). We then evaluate the model on a new testing dataset of 8 different protocols tested across 40 cells (see Note S1 and Table S1).

RESULTS

Performance of the hierarchical Bayesian model

We adopt the HBM approach to predict the lifetime of new cycling protocols. For ease of presentation, let us first consider the case of classifying batteries into $k = 2$

Table 1. Testing results for protocol-lifetime prediction by HBM with one sample observed for the cases of k = 2, 3, 4, 5, and 6 groups

	k = 2	k = 3	k = 4	k = 5	k = 6
RMSE (cycles)	85.3	58.7	63.8	59.6	62.3
Average percent error	8.1%	5.7%	6.5%	6.3%	6.3%

The degree of lifetime variability mean(α) for k = 2, 3, 4, 5, and 6 are mean(α) = 0.07, 0.11, 0.12, 0.12, and 0.18, respectively, (see Figures S5–S8 for more details).

groups according to their lifetime (long life/short life threshold = 900 cycles). The degree of lifetime variability within the training data estimated by HBM is mean(α) = 0.09, and the average lifetime distribution across all training protocols is mean($\boldsymbol{\beta}$) = [0.52, 0.48]. As shown in the left plot of Figures S4A and S4B, we apply HBM to estimate the lifetime distribution (i.e., the predicted probability distribution of short-lived $p(\boldsymbol{\theta}[1]|\, \boldsymbol{y}^{new})$ and long-lived $p(\boldsymbol{\theta}[2]|\, \boldsymbol{y}^{new})$ batteries) of batteries tested with a new cycling protocol after only one battery is tested and observed as being either short lived ($\boldsymbol{y}^{new}$ = [1,0]) or long lived ($\boldsymbol{y}^{new}$ = [0,1]), where $\boldsymbol{\theta}[j],\ j = \boldsymbol{1},\ \boldsymbol{2}$ are the proportions of batteries in group 1 (short lived) and group 2 (long lived) generated from a new protocol, respectively, and $\boldsymbol{y}^{new}$ indicates a set of observations of battery lifetime from a new protocol (for more details on symbol definition, see computational). The expected fraction of long-lived and short-lived batteries can then be computed (e.g., $p(\boldsymbol{\theta}[j]>\boldsymbol{0.5}\ |\boldsymbol{y}^{new})$, as shown in the right plot of Figures S4A and S4B). We thereby estimate the cycle life of a new protocol based on Equation 10. After cycling only one battery to failure with a new protocol (i.e., $\boldsymbol{y}^{new}$ = [1,0] or [0,1]), the HBM approach obtains high protocol prediction performance, with a testing average percent error of 8.1% for protocol-lifetime prediction for LFP/graphite cells in the scenario of k = 2 groups (see Table 1). Take the case of the long life/short life threshold of 900 cycles as an example, as shown in Figure S4. After observing one battery as being long lived (>900 cycles) after cycling with a new cycling protocol (i.e., $\boldsymbol{y}^{new}$ = [0,1]), HBM possesses 25.9% and 74.1% degree of confidence to predict this protocol belonging to short-lifetime protocol group (i.e., $p(\boldsymbol{\theta}[\boldsymbol{1}]>\boldsymbol{0.5})$ = 25.9%) and long-lifetime protocol group (i.e., $p(\boldsymbol{\theta}[\boldsymbol{2}]>\boldsymbol{0.5})$ = 74.1%), respectively. Therefore, the cycle life of this protocol can be computed as 929 cycles according to Equation 10. Similarly, after observing only one battery as being short lived (i.e., $\boldsymbol{y}^{new}$= [1,0]), HBM possesses 78.0% and 22.0% degree of confidence to predict this protocol into short-lifetime protocol group (i.e., $p(\boldsymbol{\theta}[\boldsymbol{1}]>\boldsymbol{0.5})$ = 78.0%) and long-lifetime protocol group (i.e., $p(\boldsymbol{\theta}[\boldsymbol{2}]$ >0.5) = 22.0%), and the protocol's lifetime can be estimated as 751 cycles according to Equation 10.

We also consider prediction of the lifetime of cycling protocols in the contexts of multiple (i.e., k > 2) equal-range groups. The protocol-lifetime prediction results for k = 3, 4, 5, and 6 (the specific battery lifetime groups for the cases of k = 3, 4, 5, and 6 are (1) k = 3 case: lifetime groups = (500, 750](750, 1,000](1,000, ∞), (2) k = 4 case: lifetime groups = (500, 700](700, 900](900, 1,100](1,100, ∞), (3) k = 5 case: lifetime groups = (500, 650](650, 800](800, 950](950, 1,100](1,100, ∞), and (4) k = 6 case: lifetime groups = (500, 600](600, 700](700, 800](800,900](900,1,000](1,000, ∞)) (corresponding to group ranges = 250, 200, 150, and 100 cycles, respectively) are provided in Table 1, according to Equation 10. For the cases of k = 3, 4, 5, and 6 groups, after observing only one sample, the proposed HBM approach obtained overall protocol prediction performance with 6.2% of average percent error based on the testing data (see Table 1; Figure S3).

The comparison of HBM with a benchmarking single-level model[21] is provided in Table S2, which shows that the average percent error of benchmarking single-level

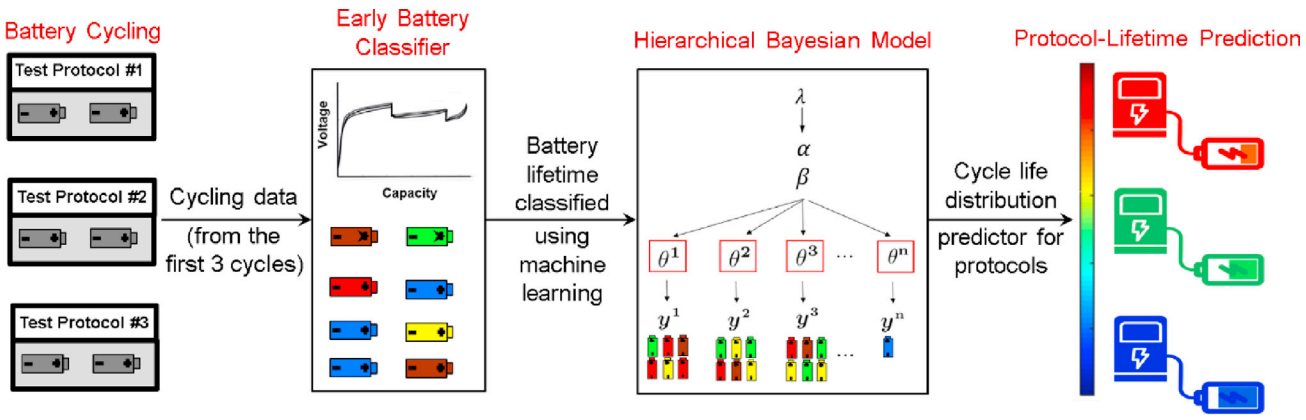

Figure 3. Schematic of the combined battery lifetime early prediction model with the hierarchical Bayesian approach for cycling protocol-lifetime prediction

Electrochemical cycling data are collected for lithium-ion batteries for a variety of cycling protocols. Then features based on the cycle-to-cycle evolution of charge $V(Q)$ are constructed from the data from the first 3 cycles. Additional features can be included if additional data are available, such as temperature. The features and data are used to construct a battery lifetime prediction model, whose predictions are used to construct a hierarchical Bayesian model for predicting the battery cycle-life distribution when fed new cycling protocols.

method is a factor of 1.7 higher than the overall average percent error of HBM (6.5% for HBM versus 11.0% for single-level model). Our model leverages higher order knowledge abstracted from previously learned protocols to infer a new cycling protocol's performance, as well as an appropriate similarity metric from only few samples.[21,22]

Performance of combined HBM and battery lifetime prediction model

Having demonstrated the efficacy of the HBM in predicting protocol lifetimes after observing the lifetime of only a single battery with a new protocol, this section applies the HBM to battery lifetime data predicted from early-cycle information (see Figure 3). This approach enables prediction of new protocols without the need to cycle a battery to failure, thereby substantially reducing the testing time required for protocol prediction. Severson et al.[2] demonstrated accurate battery lifetime prediction using machine learning techniques applied to a wide variety of electrochemical features, with a high predictability obtained using a single feature involving the change in discharging capacity-versus-voltage profile between cycles, which is referred to as "ΔQ." It was pointed out that the ΔQ features constructed based on constant current discharging capacity-voltage data are hard to apply in a practical situation, where a cell's discharge current frequently changes to meet the user's operations. Here, we generate new features for the data-driven model—termed ΔV features (see Note S3)—that have comparable performance as ΔQ for constant current cycling data, while also performing well for variable current cycling data. The variable current refers to the fact that values of current can change within each charging cycle. For each battery, the cycling data are generated by repeating same cycling protocol, which results in time variation in the current near the end of the charging, as the capacity fades. Further, these new charging features offer a straightforward and direct connection to standard electrochemical theory in which the spatiotemporal distribution of overpotentials dictates the dynamics and condition of the battery (for more details, see the discussion in physical interpretation on predictive ability of ΔV features).

Using all twenty features, including the charging ΔV features and features similar to those in Severson et al.[2] computed for data from the first 3 cycles (the features are detailed in

Note S3), we employ a regularized minimax probability machine,[30,31] which is a distribution-free technique that does not assume any specific form of data distribution, to classify batteries into either "short-lived" or "long-lived" battery groups for various cycle-life thresholds. This method attained a test error of 12.5%, that is, with 5 of 40 points incorrectly classified for the testing dataset of LFP/graphite cells (for more details, see Note S4). Then HBM is performed on the data of these predicted LFP/graphite battery lifetimes, which achieves a test average percent error of 8.8% for protocol-lifetime prediction, after observing only one sample of a new cycling protocol. In contrast, the benchmarking single-level model[21] is performed on the data of these predicted battery lifetimes from using all the twenty features, which obtains a test error of 18.2% for protocol-lifetime prediction after one measurement of a new protocol (see Note S2). The protocol-lifetime prediction by the benchmarking method is a factor of 2.1 higher than the average percent error of HBM.

In addition, the combined HBM and battery lifetime prediction approach is applied to a dataset with a different battery chemistry (NMC/graphite)[32] than LFP/graphite. The results of the correlation analysis between the charging ΔV feature with battery lifetime, and the proposed HBM-based model for the prediction of cycling protocol-lifetime for NMC/graphite batteries are provided in Figures S12 and S13 and Table S6. The proposed charging ΔV feature has good correlation performance with the battery cycle life (the correlation coefficient is -0.88 as shown in Figure S12). In addition, HBM is performed on the data of the NMC/graphite battery lifetimes predicted from the first 3 cycles (see Figure S13), which achieves a test average percent error of 10.4% for protocol-lifetime prediction using a single 3-cycle test. In contrast, the benchmarking single-level model[21] is performed on the data of these predicted battery lifetimes, which obtains a test error of 20.2% for protocol-lifetime prediction after one measurement. The proposed HBM approach provides a factor of 1.94 higher accuracy in protocol-lifetime prediction than the benchmarking single-level prediction method. The results show the effectiveness of the proposed approach for cycling protocol prediction when applying the method to a battery dataset with a chemistry other than LFP/graphite. The above-mentioned results also show that the combination of HBM and a data-driven battery lifetime prediction model (minimax probability machine) enables rapid and accurate protocol prediction using only battery lifetimes predicted from very early-cycle information, substantially reducing both experimental costs (the number of batteries) and testing time.

DISCUSSION

HBM prediction from few observations

This section investigates the relationship between the number of observations (n) and the cell-to-cell variability degree (α) for the HBM-based protocol classification performance according to the decision rule of Equation 9. When the variability degree α is small (e.g., α is near 0, see the uniform lifetime case in Figure 1A), the first observation would indicate the (nearly, deterministically correct) answer; therefore, there is much to be gained from one observation, but subsequent observations are of little use. As the variability degree α increases, more observations would be needed to make the predicted distribution become accurate. Figure 4 plots the predicted performance of HBM as a function of observation number (n) and the cell-to-cell variability degree (α) for the case of classifying cycling protocols into two protocol groups. As shown in Figures 4A and 4F, the majority of prediction accuracy is gained with the first few observations, and subsequent observations do little to improve performance. Therefore, HBM provides a way of quantifying the marginal gain in confidence for prediction from additional experiments.

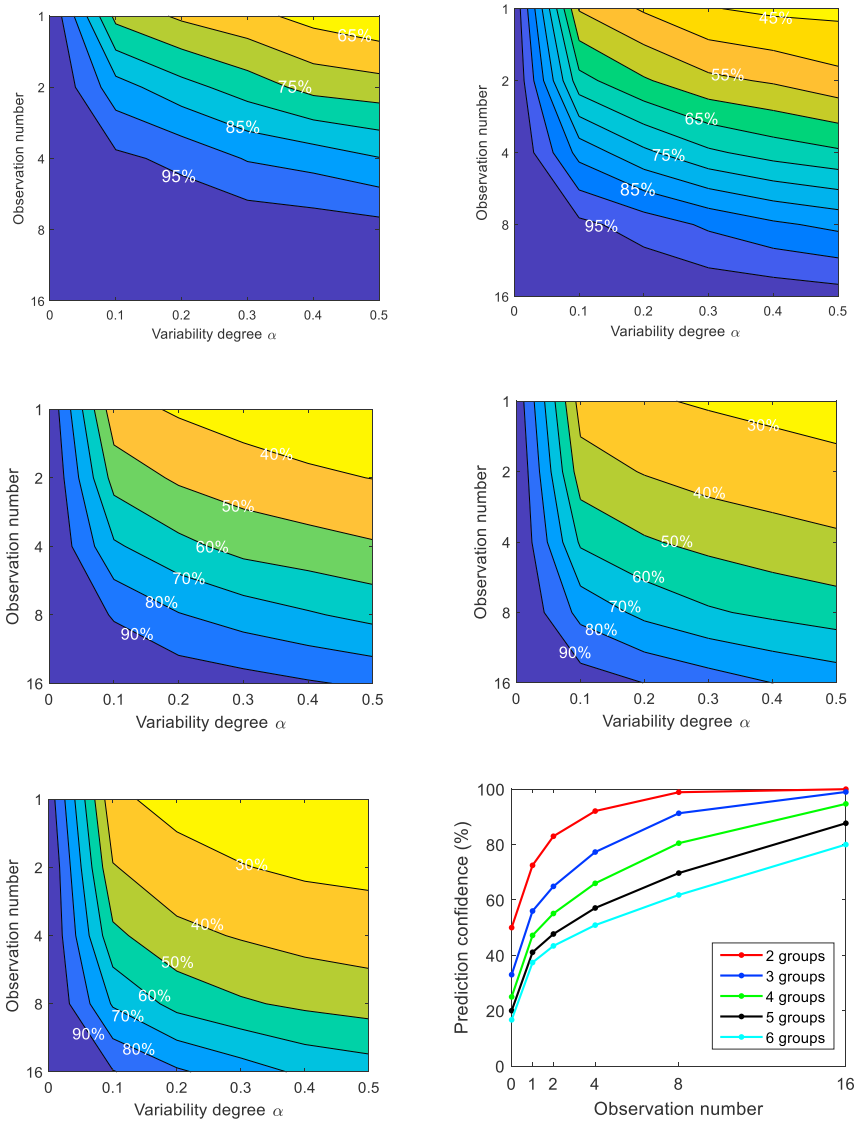

Figure 4. Classification performance of HBM as a function of observation number (*n*) and the cell-to-cell variability degree (α) for the case of classifying cycling protocols into multiple-protocol groups

(A–F) (A) k = 2 groups, (B) k = 3 groups, (C) k = 4 groups, (D) k = 5 groups, (E) k = 6 groups, and (F) prediction confidence of HBM as a function of observation number for the cases of k = 2, 3, 4, 5, and 6 groups; in each case, the prediction confidence is computed by averaging the values of prediction confidence for the variability degree α= 0, 0.1, 0.2, 0.3, 0.4, and 0.5 under the same number of observation. The labels inside the contour plot are prediction confidences (e.g., 95% means the 95% degree of confidence predicted by HBM). The result is based on simulation data.

In terms of the scenario for classifying cycling protocols into multiple (i.e., $k > 2$) groups, Figures 4B–4E depicts the predicted performance of HBM as a function of observation number (n) and the cell-to-cell variability degree (α) for classifying protocols into k = 3, 4, 5, and 6 groups, respectively. Again, similar to the case of two-group protocol classification, the advantage of many observations decreases quickly for protocol classification into multiple groups, as shown in Figure 4F.

In our specific operating window (commercial high-rate cylindrical cells cycled under fast-charging conditions), the cell-to-cell variability is between 0.07 and 0.18;

therefore, the majority of learning is achieved with a single observation. However, under different scenarios, such as high energy (thick electrode) cells cycled at high temperature, high cycling cutoff voltages, and high rates, as well as during battery development, cell-to-cell variability is larger and HBM provides more useful guidance for determining an appropriate number of repeat measurements for accurate protocol classification and prediction.

Quantification of uncertainties using HBM

This section explores the information that the HBM learns about the expected lifetime distributions for cycling protocols in the context of warranty. For example, when we have two "good" cycling protocols but predict one to have 90% of batteries be long lived and another to have 95% of batteries be long lived, this information can inform warranty decisions. In this regard, a key question arises: what is the relationship between the number of observations, the cell-to-cell variability, and the confidence in the distribution of lifetimes predicted by HBM?

We first consider the case where we seek to ensure that at least 90% of the batteries cycled with a given protocol fall within the long-lifetime range (i.e., $\boldsymbol{\theta}[2] \geq 0.9$—note that the analysis can be easily extended to other cases e.g., $\boldsymbol{\theta}[2] \geq 0.95$ or $\boldsymbol{\theta}[2] \geq 0.99$). As mentioned, the accuracy of predictions made by HBM also depends on the degree of cell-to-cell variability, α. Take $\alpha = 0.1$ as an example, as displayed in Figure S10, the number of observations (n) needed for HBM to predict a good cycling protocol having the ratio of long-lived battery $\boldsymbol{\theta}[2] \geq 0.9$ with $\eta =$ 95% degree of confidence is n = 29; that is, the prediction performance $p(\boldsymbol{\theta}[2] \geq 0.9) = 95\%$ can be guaranteed for such cycling protocols with the observations $\boldsymbol{y} = [0, n] = [0, 29]$.

In addition, for the scenarios of cell-to-cell variability degree $\alpha = 0, 0.1, 0.2, 0.3, 0.4$, and 0.5, the number of observations needed for HBM to predict cycling protocols $p(\boldsymbol{\theta}[2] \geq 0.9) = \eta$ with $\eta = 85\%, 90\%, 95\%, 99.5\%$ degree of confidence is in Figure 5. The number of observations ($y = [0, n]$) required is seen to have a log-linear relationship with the predicted degree of confidence η for HBM; in other words, as the degree of confidence η increases, the number of observations required for HBM to ensure good cycling protocols increases approximately proportional to e^{η}. The quantification of η enables predictions of pre-threshold failure rates, which enables the cost of a warranty for a given cycle-life threshold to be accurately predicted with explicit consideration of cell-to-cell variability observed in training data. Such an approach could be particularly useful in the case of reselling used batteries,[33] where the variability in lifetime (α) is large and warranties are essential for consumer confidence.

Physical interpretation on predictive ability of ΔV features

To capture the electrochemical evolution of individual cells during cycling, several features are calculated based on the cycle-to-cycle evolution of the charging voltage curve $V(Q)$ (see Figure 6A). This section explains *why* such features would be expected to be accurate predictors of battery cycle life; the features are strongly correlated to the battery degradation mechanisms that result in the capacity fade. Developing a physical interpretation of these features can guide the development of insights into the degradation mechanisms that result in the capacity reduction and provides confidence into the generalizability of the features to batteries of different chemistries or materials. Because charging voltage curves contain rich information about degradation processes especially in the graphite anode,[34] we consider here the change in charging voltage curve between cycles a and b, denoted $\Delta V_{a \to b}(Q) = V_b(Q) - V_a(Q)$, where the subscripts

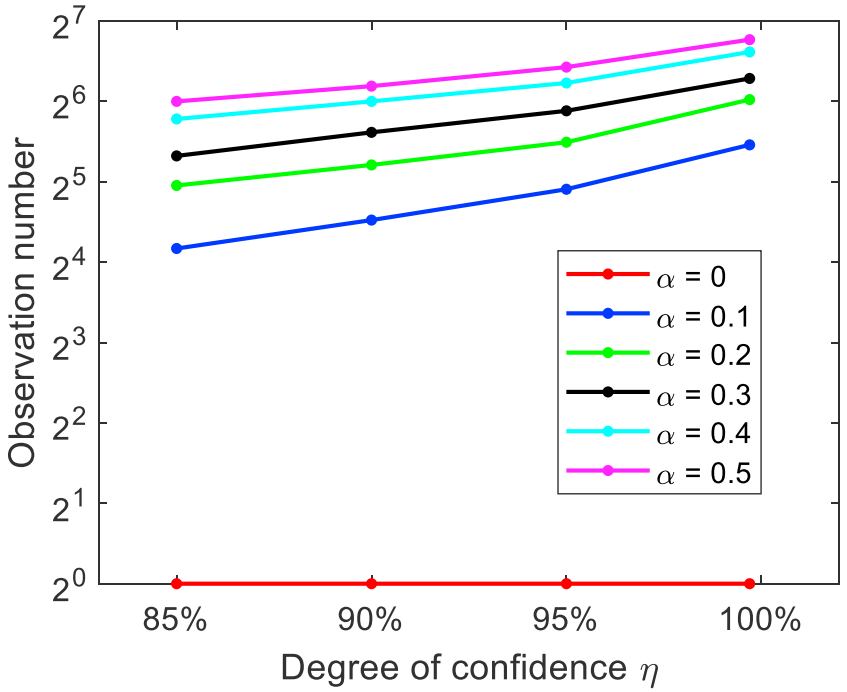

Figure 5. The number of observations needed (vertical axis) for HBM to predict the performance of cycling protocols with η = 85%, 90%, 95%, 99.5% degree of confidence (horizontal axis) with different variability degree α (different lines)

All of the numbers of observations in the figure are less than 100.

indicate the cycle number. We calculated the $\Delta V(Q)$ curves for each cell by using summary statistics, such as minimum, variance, and mean of square (see Note S3). As shown in Figure 6B, the summary statistic of mean of square, applied to $\Delta V_{30\rightarrow100}(Q)$, has a high correlation with the cycle life of a cell. In addition, the charging ΔV feature (i.e., mean(square($\Delta V_{2\rightarrow3}(Q)$))) was selected as the most predictive feature for early classification of battery lifetime (see Note S4). These results demonstrate the prediction power of the features constructed based on the differences of charging voltage curves $\Delta V(Q)$.

Under constant current scenarios, physically, the voltage difference $\Delta V_{a\rightarrow b}$ between two given cycles *a* and *b* is significantly correlated with internal resistance buildup between the two cycles at the same composition and temperature. Since there are transient effects of transport and reaction kinetics within each cycle, it is also important to assess the cumulative effect of variable differential resistance via the total energy dissipation, whose change from cycle-to-cycle is given by the total area between the voltage curves, $\Delta E_{a\rightarrow b} = \oint V(Q)\, dQ$. The statistics introduced earlier (mean, variance, and mean of square) can be viewed as different measures of the charge-resolved voltage change, corresponding to different weighted averages of the change in energy dissipation. Changes in cell resistance or energy dissipation over time can occur due to a variety of degradation phenomena, typically associated with one or both of the electrodes, which impede lithium-ion transport or intercalation reactions. Irreversible side reactions or leakage mechanisms that lead to loss of lithium-ion inventory (LLI) in the system can also indirectly affect these resistances, while shifting the open circuit voltage and lowering the total capacity.

Electrochemical side reactions at both electrodes play important roles in battery degradation, which may explain some of our findings. In order to maximize energy

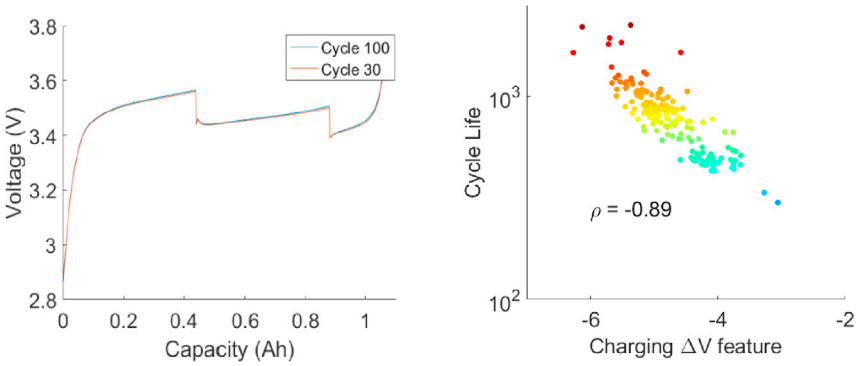

Figure 6. Charging ΔV feature of LFP/graphite cells

(A) Charging voltage curve for 100th and 30th cycles for a representative LFP/graphite cell.

(B) Cycle life plotted as a function of the charging ΔV feature of LFP/graphite cells, which is defined as the mean of square of $\Delta V_{30\rightarrow100}(Q)$, with a correlation coefficient of −0.89.

density, the operating voltage of most lithium-ion batteries lies far outside the electrochemical stability window of all battery electrolytes;[35] therefore, organic battery electrolytes are designed to form passivation layers on the active electrode surfaces, known as the solid-electrolyte interphase (SEI). In the first few cycles, primary SEI growth on carbon-based anodes, such as graphite, is rapid and occurs mainly by electron-transfer-limited solvent reduction during battery charging (lithiation).[36] As the number of cycles increases, the dense, mostly inorganic primary SEI transitions to a porous, mostly organic secondary SEI,[37] whose growth is ultimately limited by solvent diffusion.[38,39] At high charging rates, large overpotentials can also trigger lithium-plating side reactions, enhanced by graphite staging phase transitions that suppress lithium-ion intercalation,[40] which accelerate LLI and interfere with stable intercalation reactions. As the graphite capacity decreases due to LLI from all of these processes, the potential of the LFP cathode can also rise above 4.2 V (cathode overcharge).[41] Such high potentials have been shown to cause electronic structure changes in the cathode material leading to gas evolution and defect formation.[42] At the cell level, these phenomena can lead to increased interfacial resistance of charge transfer in the cathode material.[43] At both electrodes, mechanical deformation due to volume expansion and contraction during intercalation can also lead to fracture and degradation of electron transport pathways, which lower the active area over time and contribute to the growth of internal resistance.[44,45] On the cathode side, disorder also causes part of the active material to become inactive for lithium insertion.[46] In summary, the increased resistance for ion and electron transport and intercalation reactions, due to a variety of interfacial degradation processes, as well as the loss of lithium inventory and active material, leads us to expect a significant correlation of changes in $\Delta V(Q)$ statistics with battery lifetime. Moreover, the dissipation of energy as heat leads to the further expectation that greater temperature increases during charging would also correlate with greater degradation and shorter lifetimes.

EXPERIMENTAL PROCEDURES

Resource availability

Lead contact

Please contact the lead contact, R.D.B. (braatz@mit.edu) for information related to the data and code described in the following experimental procedures section.

Materials availability

This study did not generate new unique materials.

Data and code availability

The dataset of LFP/graphite cells used in this work is available at https://github.com/chueh-ermon/battery-fast-charging-optimization; and the dataset of NMC/graphite cells is available at https://www.batteryarchive.org/list.html. Code is available at https://github.com/bbjiang2021/HBMProtocolPrediction and upon request to the lead contact.

Experimental

Two battery datasets with two different battery chemistries are used in this work. The first dataset comprises 113 LFP/graphite batteries, which is a much more comprehensive dataset and is mainly used in this work; the second dataset comprises 21 NMC/graphite batteries, which is supplementary to verify the generalizability of proposed approaches to different battery chemistries.

The LFP/graphite dataset comprises 29 different fast-charging protocols (9 to 13 min to 80% state of charge [SOC]) tested across 113 commercial lithium-iron-phosphate/graphite cells (see Figure 2) from Severson et al.[2] and Attia et al.[9] The cells are of a nominal capacity of 1.1 Ah and a nominal voltage of 3.3 V. The experiments were operated at a temperature-controlled environmental chamber in which the average temperature of individual batteries spanned a temperature range of about 6°C (see Figure S16). This battery dataset is appropriate for the purposes of this study, which include (1) validating a machine learning method for the rapid prediction of the performance cycling protocols, (2) improving the predictive accuracy of the method by defining new features, aka transformations of the raw battery data. The training dataset contains 73 cells with 21 different charging protocols, and the testing dataset contains 8 fast-charging protocols with each protocol repeated five times (i.e., 40 cells for the test), as shown in Figure S2 and Table S1. Those fast charging contain multi-constant-current step protocols, and one of 29 different charging protocols was performed to charge cells from 0% to 80% SOC. For example, a three-step protocol can comprise a 4C charging step from 0% to 30% SOC, followed by a 3C step from 30% to 50% SOC and a 6C step from 50% to 80% SOC. The 29 charging protocols indicate different combinations of current steps within the range of 0% to 80% SOC. All cells are then charged from 80% to 100% SOC with a uniform 1C CC-CV charging step to 3.6 V. All cells were subsequently discharged with a CC-CV discharge at 4C to 2.0 V. The cycle life defined here is the cycle number corresponding to the cell capacity reducing to 80% of its nominal capacity. More details can be found in Severson et al.[2] and Attia et al.[9] on the experimental implementation for the LFP/graphite battery dataset.

The NMC/graphite dataset comprises 21 commercial cells from Preger et al.[32] The 21 cells were cycled at various ambient temperatures (15°C, 25°C, and 35°C). On each cycle, the cells were charged in a CCCV (Constant Current Constant Voltage) mode at 0.5C constant current up to 4.2 V, followed by a constant voltage charge. The cells were then discharged at various discharge currents (0.5C, 1C, 2C, and 3C) until the terminal voltage decreased to 2 V. The capacity versus cycle number for an NMC/graphite battery dataset is plotted in Figure S11, and a detailed description of the dataset is available in Preger et al.[32]

Computational

This section formalizes the HBM in Figure 1, which is known as a Dirichlet-multinomial model.[47] Consider a set of k groups. For ease of presentation, variables are initially defined for the case of $k = 2$. The variables for the case of $k > 2$ can be defined similarly. Let $\boldsymbol{\theta}^i$ indicate the true battery lifetime distribution for the ith cycling protocol: if 30% of

the batteries from protocol 4 are short lived, then $\boldsymbol{\theta}^4$ = [0.3, 0.7]. Let $\boldsymbol{y}^i$ indicate a set of observations of battery lifetime from protocol i. If six samples are drawn from protocol 4 and all batteries but one sample is short lived, then $\boldsymbol{y}^4$ = [5, 1].

Suppose we observe the lifetime data from cycling protocols $\boldsymbol{y} = \{\boldsymbol{y}^1, \boldsymbol{y}^2, \ldots\}$, where $\boldsymbol{y}^i$, $i = 1, 2, \ldots$, is the data observations of battery lifetime from protocol i. We assume that $\boldsymbol{y}^i$ is drawn from a multinomial distribution with parameter $\boldsymbol{\theta}^i$; in other words, the battery lifetimes responsible for the observations in$\boldsymbol{y}^i$are drawn independently at random from the *i*th protocol, and each lifetime data depends on the lifetime distribution $\boldsymbol{\theta}^i$ for that protocol. Therefore, the likelihood can be expressed as

$$p(\boldsymbol{y}) = \prod_i p(\boldsymbol{y}^i | n^i) \quad \text{(Equation 1)}$$

and

$$p(\boldsymbol{y}^i | n^i) \sim \text{Multinomial}(\boldsymbol{\theta}^i) \quad \text{(Equation 2)}$$

where n^i is the number of observations for protocol *i*.

The vectors $\boldsymbol{\theta}^i$, $i = 1, 2, \ldots$, are assumed to be drawn from a Dirichlet distribution parameterized by a vector $\boldsymbol{\gamma} = [\gamma_1, \gamma_2, \ldots, \gamma_k]^T$, which is described as follows:[47]

$$p(\boldsymbol{\theta}^i) \sim \text{Dir}(\boldsymbol{\theta}|\boldsymbol{\gamma}) = \frac{1}{B(\boldsymbol{\gamma})} \prod_{j=1}^{k} \theta_j^{\gamma_j - 1} \quad \text{(Equation 3)}$$

where

$$B(\boldsymbol{\gamma}) \triangleq \prod_{j=1}^{k} \Gamma(\gamma_j) / \Gamma(\gamma_0) \quad \text{(Equation 4)}$$

and

$$\gamma_0 \triangleq \sum_{j=1}^{k} \gamma_j \quad \text{(Equation 5)}$$

For the definitions

$$\alpha = \gamma_0 \Big/ k = \sum_{j=1}^{k} \gamma_j / k \quad \text{(Equation 6)}$$

and

$$\boldsymbol{\beta} = [\beta_1, \beta_2, \ldots, \beta_k]^T \text{ with } \beta_j = \gamma_j \Big/ \gamma_0, \quad \text{(Equation 7)}$$

the parameter α indicates the overall degree of cell-to-cell lifetime variability among different cycling protocols, and $\boldsymbol{\beta}$ represents the distribution of lifetime across the entire collection of protocols.[22,21] As in past HBM applications,[21] we initialized the algorithm by an exponential distribution on α and a uniform distribution on $\boldsymbol{\beta}$, where the latter captures the weak prior expectation that the batteries from any cycling protocol are uniform in lifetime. The mean of the exponential distribution is λ, and λ = 1 is used in this paper.

The posterior distribution $p(\alpha, \boldsymbol{\beta}, \{\boldsymbol{\theta}^i\} | \boldsymbol{y})$ (or $p(\boldsymbol{\gamma}, \{\boldsymbol{\theta}^i\} | \boldsymbol{y})$) can be obtained through multiplying the likelihood (i.e., Equation 1) by the prior (i.e., Equation 3).[47] The objective is to maximize the posterior distribution $p(\alpha, \boldsymbol{\beta}, \{\boldsymbol{\theta}^i\} | \boldsymbol{y})$ to simultaneously learn level-2 knowledge about α and $\boldsymbol{\beta}$ and level-1 knowledge about the lifetime distribution $\boldsymbol{\theta}^i$ of each individual protocol i. To compute the predictions of this model, we estimate $p(\alpha, \boldsymbol{\beta} | \boldsymbol{y})$ using the Markov chain Monte Carlo method.[47] Inferences about the $\boldsymbol{\theta}^i$ are computed by integrating over α and $\boldsymbol{\beta}$:

$$p(\boldsymbol{\theta}^i | \boldsymbol{y}) = \int_{\alpha, \boldsymbol{\beta}} p(\boldsymbol{\theta}^i | \alpha, \boldsymbol{\beta}, \boldsymbol{y}) p(\alpha, \boldsymbol{\beta} | \boldsymbol{y}) \mathrm{d}\alpha \mathrm{d}\boldsymbol{\beta} \quad \text{(Equation 8)}$$

The category of cycling protocol i can be classified as follows:

$$j = \arg\max_{j=1,\ldots,k} \{p(\boldsymbol{\theta}^i[j] > 1/k)\} \quad \text{(Equation 9)}$$

where $p(\boldsymbol{\theta}^i[j] > 1/k)$ is the summation of all of the probabilities in which the $\boldsymbol{\theta}^i[j]$ are larger than $1/k$, and k is the division number of lifetime groups. The cycle life of cycling protocol i can be calculated as follows:

$$\hat{z}_i = \sum_{j=1}^{k} p(\boldsymbol{\theta}^i[j] > 1/k) \times m_j \quad \text{(Equation 10)}$$

where $\hat{z}_i$ is the estimated cycle life of the ith protocol and m_j is the median cycle life of the jth lifetime group.

The metrics of average percent error and root-mean-squared error (RMSE) are used to evaluate the model performance. The average percent error is defined as follows:

$$\frac{1}{N}\sum_{i=1}^{N}\frac{|z_i - \hat{z}_i|}{z_i} \times 100 \quad \text{(Equation 11)}$$

where z_i is the mean of observed cycle life of ith protocol from multiple experiments and N is the total number of tested protocols. RMSE is defined as

$$\text{RMSE} = \sqrt{\frac{1}{N}\sum_{i=1}^{N}(z_i - \hat{z}_i)^2} \quad \text{(Equation 12)}$$

SUPPLEMENTAL INFORMATION

Supplemental information can be found online at https://doi.org/10.1016/j.joule.2021.10.010.

ACKNOWLEDGMENTS

This work was supported by Toyota Research Institute through the Accelerated Materials Design and Discovery program. B.J. was sponsored by Tsinghua-Toyota Joint Research Fund. S.J.H. was supported by the Assistant Secretary for Energy Efficiency, Vehicle Technologies Office of the U.S. Department of Energy under the Advanced Battery Materials Research Program.

AUTHOR CONTRIBUTIONS

B.J. and F.M. carried out the modeling. B.J. and M.F. developed and H.Z. explained the new features. B.J. and W.E.G. performed HBM for warranty considerations. P.K.H. performed data management and provided input on the initial analysis. B.J., W.E.G., M.D.B., S.D., M.Z.B., S.J.H., W.C.C., and R.D.B. interpreted the results. All authors edited and reviewed the manuscript. R.D.B. supervised the work.

DECLARATION OF INTERESTS

A coauthor is employed by Toyota Research Institute, which financially supported this research. A patent application has been submitted based on this work.

Received: March 26, 2021
Revised: May 17, 2021
Accepted: October 4, 2021
Published: October 29, 2021

REFERENCES

1. Cano, Z.P., Banham, D., Ye, S., Hintennach, A., Lu, J., Fowler, M., and Chen, Z. (2018). Batteries and fuel cells for emerging electric vehicle markets. Nat. Energy *3*, 279–289.
2. Severson, K.A., Attia, P.M., Jin, N., Perkins, N., Jiang, B., Yang, Z., Chen, M.H., Aykol, M., Herring, P.K., Fraggedakis, D., et al. (2019). Data-driven prediction of battery cycle life before capacity degradation. Nat. Energy *4*, 383–391.
3. Waag, W., Fleischer, C., and Sauer, D.U. (2014). Critical review of the methods for monitoring of lithium-ion batteries in electric and hybrid vehicles. J. Power Sources *258*, 321–339.
4. Dunn, B., Kamath, H., and Tarascon, J.-M. (2011). Electrical energy storage for the grid: a battery of choices. Science *334*, 928–935.
5. Schmuch, R., Wagner, R., Hörpel, G., Placke, T., and Winter, M. (2018). Performance and cost of materials for lithium-based rechargeable automotive batteries. Nat. Energy *3*, 267–278.
6. Anseán, D., González, M., Viera, J.C., García, V.M., Blanco, C., and Valledor, M. (2013). Fast charging technique for high power lithium iron phosphate batteries: A cycle life analysis. J. Power Sources *239*, 9–15.
7. Ahmed, S., Bloom, I., Jansen, A.N., Tanim, T., Dufek, E.J., Pesaran, A., Burnham, A., Carlson, R.B., Dias, F., Hardy, K., et al. (2017). Enabling fast charging – a battery technology gap assessment. J. Power Sources *367*, 250–262.
8. Yang, X.-G., and Wang, C.-Y. (2018). Understanding the trilemma of fast charging, energy density and cycle life of lithium-ion batteries. J. Power Sources *402*, 489–498.
9. Attia, P.M., Grover, A., Jin, N., Severson, K.A., Markov, T.M., Liao, Y.-H., Chen, M.H., Cheong, B., Perkins, N., Yang, Z., et al. (2020). Closed-loop optimization of fast-charging protocols for batteries with machine learning. Nature *578*, 397–402.
10. An, S.J., Li, J., Du, Z., Daniel, C., and Wood, D.L., III (2017). Fast formation cycling for lithium ion batteries. J. Power Sources *342*, 846–852.
11. Liu, Y., Zhu, Y., and Cui, Y. (2019). Challenges and opportunities towards fast-charging battery materials. Nat. Energy *4*, 540–550.
12. Zhang, C., Jiang, J., Gao, Y., Zhang, W., Liu, Q., and Hu, X. (2017). Charging optimization in lithium-ion batteries based on temperature rise and charge time. Appl. Energy *194*, 569–577.
13. Baumhöfer, T., Brühl, M., Rothgang, S., and Sauer, D.U. (2014). Production caused variation in capacity aging trend and correlation to initial cell performance. J. Power Sources *247*, 332–338.
14. Segler, M.H.S., Preuss, M., and Waller, M.P. (2018). Planning chemical syntheses with deep neural networks and symbolic AI. Nature *555*, 604–610.
15. Butler, K.T., Davies, D.W., Cartwright, H., Isayev, O., and Walsh, A. (2018). Machine learning for molecular and materials science. Nature *559*, 547–555.
16. Brandt, R.E., Kurchin, R.C., Steinmann, V., Kitchaev, D., Roat, C., Levcenco, S., Ceder, G., Unold, T., and Buonassisi, T. (2017). Rapid photovoltaic device characterization through Bayesian parameter estimation. Joule *1*, 843–856.
17. Tabor, D.P., Roch, L.M., Saikin, S.K., Kreisbeck, C., Sheberla, D., Montoya, J.H., Dwaraknath, S., Aykol, M., Ortiz, C., Tribukait, H., et al. (2018). Accelerating the discovery of materials for clean energy in the era of smart automation. Nat. Rev. Mater. *3*, 5–20.
18. Correa-Baena, J.-P., Hippalgaonkar, K., Van Duren, J., Jaffer, S., Chandrasekhar, V.R., Stevanovic, V., Wadia, C., Guha, S., and Buonassisi, T. (2018). Accelerating materials development via automation, machine learning, and high-performance computing. Joule *2*, 1410–1420.
19. Jain, A., Ong, S.P., Hautier, G., Chen, W., Richards, W.D., Dacek, S., Cholia, S., Gunter, D., Skinner, D., Ceder, G., and Persson, K.A. (2013). Commentary: the materials project: a materials genome approach to accelerating materials innovation. APL Mater *1*, 011002.
20. Sendek, A.D., Yang, Q., Cubuk, E.D., Duerloo, K.-A.N., Cui, Y., and Reed, E.J. (2017). Holistic computational structure screening of more than 12000 candidates for solid lithium-ion conductor materials. Energy Environ. Sci. *10*, 306–320.
21. Kemp, C., Perfors, A., and Tenenbaum, J.B. (2007). Learning overhypotheses with hierarchical Bayesian models. Dev. Sci. *10*, 307–321.
22. Tenenbaum, J.B., Kemp, C., Griffiths, T.L., and Goodman, N.D. (2011). How to grow a mind: statistics, structure, and abstraction. Science *331*, 1279–1285.
23. Salakhutdinov, R., Tenenbaum, J.B., and Torralba, A. (2012). One-shot learning with a hierarchical nonparametric Bayesian model. Proceedings of the ICML Workshop on Unsupervised and Transfer Learning, 195–206.
24. Lake, B.M., Salakhutdinov, R., and Tenenbaum, J.B. (2015). Human-level concept learning through probabilistic program induction. Science *350*, 1332–1338.
25. Perfors, A., and Tenenbaum, J.B. (2009). Learning to learn categories. In Proceedings of the 31st Annual Conference of Cognitive Science Society, pp. 136–141.
26. Fernald, A., Perfors, A., and Marchman, V.A. (2006). Picking up speed in understanding: speech processing efficiency and vocabulary growth across the 2nd year. Dev. Psychol. *42*, 98–116.
27. Griffiths, T.L., Chater, N., Kemp, C., Perfors, A., and Tenenbaum, J.B. (2010). Probabilistic models of cognition: exploring representations and inductive biases. Trends Cogn. Sci. *14*, 357–364.
28. Shafto, P., Kemp, C., Mansinghka, V., Gordon, M., and Tenenbaum, J.B. (2006). Learning cross-cutting systems of categories. Proceedings of the 28th Annual Conference of Cognitive Science Society, 2146–2151.
29. Semmens, B.X., Ward, E.J., Moore, J.W., and Darimont, C.T. (2009). Quantifying inter- and intra-population niche variability using hierarchical Bayesian stable isotope mixing models. PLoS One *4*, e6187.
30. Huang, K., Yang, H., King, I., Lyu, M.R., and Chan, L. (2004). The minimum error minimax probability machine. J. Mach. Learn. Res. *5*, 1253–1286.
31. Lanckriet, G.R., Ghaoui, L.E., Bhattacharyya, C., and Jordan, M.I. (2003). A robust minimax approach to classification. J. Mach. Learn. Res. *3*, 555–582.
32. Preger, Y., Barkholtz, H.M., Fresquez, A., Campbell, D.L., Juba, B.W., Romàn-Kustas, J., Ferreira, S.R., and Chalamala, B. (2020). Degradation of commercial lithium-ion cells as a function of chemistry and cycling conditions. J. Electrochem. Soc. *167*, 120532.
33. Cready, E., Lippert, J., Pihl, J., Weinstock, I., Symons, P., and Jungst, R.G. (2003). Final Report Technical and Economic Feasibility of Applying Used EV Batteries in Stationary Applications (Sandia National Laboratory). https://digital.library.unt.edu/ark:/67531/metadc735442/.
34. Han, X., Feng, X., Ouyang, M., Lu, L., Li, J., Zheng, Y., and Li, Z. (2019). A comparative study of charging voltage curve analysis and state of health estimation of lithium-ion batteries in electric vehicle. Automot. Innov. *2*, 263–275.
35. Goodenough, J.B., and Kim, Y. (2010). Challenges for rechargeable Li batteries. Chem. Mater. *22*, 587–603.
36. Das, S., Attia, P.M., Chueh, W.C., and Bazant, M.Z. (2019). Electrochemical kinetics of SEI growth on carbon black: part II. Modeling. J. Electrochem. Soc. *166*, E107–E118.
37. Huang, W., Attia, P.M., Wang, H., Renfrew, S.E., Jin, N., Das, S., Zhang, Z., Boyle, D.T., Li, Y., Bazant, M.Z., et al. (2019). Evolution of the solid–electrolyte interphase on carbonaceous anodes visualized by atomic-resolution cryogenic electron microscopy. Nano Lett *19*, 5140–5148.
38. Pinson, M.B., and Bazant, M.Z. (2013). Theory of SEI formation in rechargeable batteries: capacity fade, accelerated aging and lifetime prediction. J. Electrochem. Soc. *160*, A243–A250.
39. Horstmann, B., Single, F., and Latz, A. (2019). Review on multi-scale models of solid-electrolyte interphase formation. Curr. Opin. Electrochem. *13*, 61–69.
40. Thomas-Alyea, K.E., Jung, C., Smith, R.B., and Bazant, M.Z. (2017). In situ observation and mathematical modeling of lithium distribution within graphite. J. Electrochem. Soc. *164*, E3063–E3072.
41. Krueger, S., Kloepsch, R., Li, J., Nowak, S., Passerini, S., and Winter, M. (2013). How do

reactions at the anode/electrolyte interface determine the cathode performance in lithium-ion batteries? J. Electrochem. Soc. *160*, A542–A548.

42. Hausbrand, R., Cherkashinin, G., Ehrenberg, H., Gröting, M., Albe, K., Hess, C., and Jaegermann, W. (2015). Fundamental degradation mechanisms of layered oxide Li-ion battery cathode materials: methodology, insights and novel approaches. Mater. Sci. Eng. *192*, 3–25.

43. Guéguen, A., Streich, D., He, M., Mendez, M., Chesneau, F.F., Novák, P., and Berg, E.J. (2016). Decomposition of $LiPF_6$ in high energy lithium-ion batteries studied with online electrochemical mass spectrometry. J. Electrochem. Soc. *163*, A1095–A1100.

44. Harris, S.J., and Lu, P. (2013). Effects of inhomogeneities – nanoscale to mesoscale – on the durability of Li-ion batteries. J. Phys. Chem. C *117*, 6481–6492.

45. Mukhopadhyay, A., and Sheldon, B.W. (2014). Deformation and stress in electrode materials for Li-ion batteries. Prog. Mater. Sci. *63*, 58–116.

46. Birkl, C.R., Roberts, M.R., McTurk, E., Bruce, P.G., and Howey, D.A. (2017). Degradation diagnostics for lithium ion cells. J. Power Sources *341*, 373–386.

47. Murphy, K.P. (2012). Machine Learning: A Probabilistic Perspective (MIT Press).